

2017

Differential presynaptic ATP supply for basal and high-demand transmission

Courtney Sobieski

Washington University School of Medicine

Michael J. Fitzpatrick

Washington University School of Medicine

Steven Mennerick

Washington University School of Medicine

Follow this and additional works at: https://digitalcommons.wustl.edu/open_access_pubs

Recommended Citation

Sobieski, Courtney; Fitzpatrick, Michael J.; and Mennerick, Steven, "Differential presynaptic ATP supply for basal and high-demand transmission." *The Journal of Neuroscience*,. 2712-16. (2017).
https://digitalcommons.wustl.edu/open_access_pubs/5548

This Open Access Publication is brought to you for free and open access by Digital Commons@Becker. It has been accepted for inclusion in Open Access Publications by an authorized administrator of Digital Commons@Becker. For more information, please contact engeszer@wustl.edu.

Research Articles: Cellular/Molecular

Differential presynaptic ATP supply for basal and high-demand transmission

Courtney Sobieski^{1,4}, Michael J. Fitzpatrick^{1,5} and Steven Mennerick^{1,2,3}

^{1,2,3,4,5}*Department of Psychiatry, Neuroscience, and Taylor Family Institute for Innovative Psychiatric Research, and Graduate Program in Neuroscience, Medical Scientist Training Program, Washington University School of Medicine, St. Louis, MO 63110, United States*

DOI: 10.1523/JNEUROSCI.2712-16.2017

Received: 27 August 2016

Revised: 10 January 2017

Accepted: 13 January 2017

Published: 16 January 2017

Author contributions: C.S., M.F., and S.J.M. designed research; C.S. and M.F. performed research; C.S., M.F., and S.J.M. analyzed data; C.S., M.F., and S.J.M. wrote the paper.

Conflict of Interest: The authors declare no competing financial interests.

This work was supported by NIH grants MH078823, MH099658, MH104506, and MH106198. We thank Ann Benz and Amanda Taylor for technical help with cultures. We thank lab members for advice and discussion.

Correspondence to Steven Mennerick, Department of Psychiatry, Washington University School of Medicine, 660 S. Euclid Ave., Campus Box 8134, St. Louis, MO 63110, menneris@wustl.edu

Cite as: J. Neurosci 2017; 10.1523/JNEUROSCI.2712-16.2017

Alerts: Sign up at www.jneurosci.org/cgi/alerts to receive customized email alerts when the fully formatted version of this article is published.

Accepted manuscripts are peer-reviewed but have not been through the copyediting, formatting, or proofreading process.

Copyright © 2017 the authors

1 **Differential presynaptic ATP supply for basal and high-demand**
2 **transmission**

3
4 Courtney Sobieski^{1,4}, Michael J. Fitzpatrick,^{1,5} Steven Mennerick^{1,2,3}

5
6 Department of Psychiatry¹, Neuroscience², and Taylor Family Institute for
7 Innovative Psychiatric Research,³ and Graduate Program in Neuroscience,⁴
8 Medical Scientist Training Program⁵
9 Washington University School of Medicine
10 St. Louis, MO 63110
11 United States

12
13 Correspondence to
14 Steven Mennerick
15 Department of Psychiatry
16 Washington University School of Medicine
17 660 S. Euclid Ave., Campus Box 8134
18 St. Louis, MO 63110
19 menneris@wustl.edu

20
21
22 36 pages
23 8 Figures, 0 Tables
24 157 Abstract words, 576 Introduction words, 1396 Discussion words

25
26 **Abbreviated title:** Presynaptic ATP sources

27
28
29
30 **Acknowledgements** This work was supported by NIH grants MH078823, MH099658,
31 MH104506, and MH106198. We thank Ann Benz and Amanda Taylor for technical help
32 with cultures. We thank lab members for advice and discussion.

33
34 **Conflict of Interest.** The authors declare no competing financial interests.

35
36

37 **Abstract**

38 The relative contributions of glycolysis and oxidative phosphorylation to neuronal
39 presynaptic energy demands are unclear. In rat hippocampal neurons, ATP production
40 by either glycolysis or oxidative phosphorylation alone sustained basal evoked synaptic
41 transmission for up to 20 min. However, combined inhibition of both ATP sources
42 abolished evoked transmission. Neither action potential propagation failure nor
43 depressed Ca^{2+} -influx explained loss of evoked synaptic transmission. Rather, inhibition
44 of ATP synthesis caused massive spontaneous vesicle exocytosis, followed by arrested
45 endocytosis, accounting for the disappearance of evoked postsynaptic currents (PSCs).
46 In contrast to its weak effects on basal transmission, inhibition of oxidative
47 phosphorylation alone depressed recovery from vesicle depletion. Local astrocytic
48 lactate shuttling was not required. Instead, either ambient monocarboxylates or neuronal
49 glycolysis was sufficient to supply requisite substrate. In summary basal transmission
50 can be sustained by glycolysis, but strong presynaptic demands are met preferentially by
51 oxidative phosphorylation, which can be maintained by bulk but not local
52 monocarboxylates or by neuronal glycolysis.

53
54
55

56 **Significance Statement**

57 Neuronal energy levels are critical for proper central nervous system function, but the
58 relative roles for the two main sources of ATP production, glycolysis and oxidative
59 phosphorylation, in fueling presynaptic function is unclear. Either glycolysis or oxidative
60 phosphorylation can fuel low-frequency synaptic function, and inhibiting both underlies
61 loss of synaptic transmission via massive vesicle release and subsequent failure to
62 endocytose lost vesicles. Oxidative phosphorylation, fueled by either glycolysis or
63 endogenously released monocarboxylates, can fuel more metabolically demanding tasks
64 such as vesicle recovery after depletion. Our work demonstrates the flexible nature of
65 fueling presynaptic function to maintain synaptic function.

66 **Introduction**

67 Neurons are energetically demanding cells, requiring a staggering amount of
68 ATP to maintain ion gradients during signaling, and to power presynaptic vesicle cycling
69 and filling. Although postsynaptic function is especially demanding (Attwell and Laughlin,
70 2001; Harris et al., 2012), the energetic cost of presynaptic function has recently been
71 highlighted (Rangaraju et al., 2014; Pathak et al., 2015; Jang et al., 2016; Lujan et al.,
72 2016). With >20,000 presynaptic ATP molecules consumed per glutamate vesicle
73 (Attwell and Laughlin, 2001; Harris et al., 2012) not including ATP used for the
74 restoration of presynaptic sodium and potassium gradients, the estimated 1×10^6
75 molecules of ATP at the presynaptic terminal would be rapidly exhausted without re-
76 supply (Rangaraju et al., 2014).

77 Glucose is the predominant source of ATP in the central nervous system. After
78 crossing the blood brain barrier, glucose is utilized by neurons and astrocytes to produce
79 ATP through glycolysis and oxidative phosphorylation. Glycolysis quickly converts
80 glucose into two molecules of pyruvate and a net total of two ATP. This provides cells
81 with a rapid source of ATP for a short period of time, particularly in the absence of
82 oxygen. Mitochondrial oxidative phosphorylation produces ATP at a slower rate but has
83 a higher yield (32 ATP versus 2 produced with glycolysis; Pfeiffer et al., 2001).
84 Substrates other than metabolically derived pyruvate can also feed the TCA cycle and
85 oxidative phosphorylation. These include astrocyte-derived lactate (Schurr et al., 1988;
86 Izumi et al., 1997; Gallagher et al., 2009; Ivanov et al., 2011; Wyss et al., 2011), ketone
87 bodies (Edmond et al., 1987; Auestad et al., 1991; Izumi et al., 1998; McKenna, 2012;
88 Takahashi et al., 2014), or glutamate (Hertz et al., 1988; Sonnewald et al., 1996;
89 McKenna, 2007, 2012).

90 The relative importance of glycolysis and oxidative phosphorylation in fueling
91 presynaptic function remains unclear. Glycolysis may be particularly vital for vesicle

92 endocytosis (Rangaraju et al., 2014), localization of synaptic vesicle machinery to
93 synaptic terminals (Jang et al., 2016), and glutamate accumulation in synaptic vesicles
94 (Ikemoto et al., 2003). Recent evidence also suggests that glycolytic failure quickly alters
95 the presynaptic action potential waveform to depress transmission at the calyx of Held
96 synapse (Lujan et al., 2016). However, other studies have demonstrated a prime effect
97 of oxidative phosphorylation in powering synaptic transmission and information
98 processing (Schurr et al., 1988; Izumi et al., 1997; Ivanov et al., 2011; Wyss et al., 2011;
99 Hall et al., 2012).

100 Some of the confusion may arise because few of the above studies directly
101 queried the relative roles of glycolysis and oxidative phosphorylation on presynaptic
102 function under controlled conditions that reduce secondary explanations for transmission
103 deficits. In a reduced, controlled environment, we find that although continuous ATP
104 production is indeed important to sustain transmitter release, ablation of evoked
105 transmission requires tandem inhibition of glycolysis and oxidative phosphorylation. We
106 tracked the loss of transmission to massive vesicle exocytosis, which in the absence of
107 ATP synthesis, failed to elicit commensurate vesicle endocytosis and recovery. We also
108 found a privileged role for oxidative phosphorylation in fueling recovery of synaptic
109 transmission after rapid depolarization-induced vesicle depletion even when glycolysis
110 was inhibited, suggesting the availability of alternative substrates for oxidative
111 phosphorylation. Neurons appear to power oxidative phosphorylation with either the
112 glycolytic breakdown of glucose or the utilization of extracellular monocarboxylates,
113 presumably from surrounding astrocytes. However, inhibiting either fuel source alone did
114 not affect recovery. We conclude that evoked transmission exhibits flexibility in ATP
115 sourcing that yields resilience of presynaptic function to changes in metabolic conditions.

116

117 **Materials and Methods**

118 Hippocampal Cell Culture

119 Cell cultures were produced and maintained as previously reported (Mennerick
120 and Zorumski, 1995; Moulder et al., 2007) Briefly, hippocampal (neuron) and cortical
121 (astrocyte) tissue of postnatal day 1-4 Sprague-Dawley rat pups of both sexes (85%
122 female) were harvested using protocols approved by the Washington University Animal
123 Studies Committee. The tissue was digested by 1 mg/ml papain, and mechanically
124 dispersed. First, astrocytes were plated on collagen microcultures in Eagle's medium
125 (Life Technologies) supplemented with 5% heat-inactivated horse serum, 5% fetal
126 bovine serum, 17 mM D-glucose, 400 μ M glutamine, 500 U/ml penicillin, and 50 μ g/ml
127 streptomycin and maintained at 37°C in a humidified incubator (5% CO₂/95% air) before
128 neuronal plating. Neurons were plated at a low density (~100 cells/mm²). +/-Astrocyte
129 microcultures were prepared as previously described (Sobieski et al., 2015). Briefly, 25-
130 mm glass coverslips were stamped with a polydimethylsiloxane microstamp coated with
131 0.5 mg/ml collagen to create 150-200 μ m diameter microdots and backfilled with a non-
132 permissive substrate poly-L-lysine grafted polyethylene glycol (PLL(20 kDa)-g[3.5]-
133 PEG(2 kDa); Surface Solutions, Dübendorf, Switzerland) at a concentration of 10 μ g/ml
134 in PBS for 1 hour and then washed with 1x PBS. Unless otherwise stated, experiments
135 were performed between 9-14 days *in vitro*.

136

137 Electrophysiology

138 Whole-cell electrophysiological recordings were performed at room temperature
139 on the stage of an Eclipse TE2000-S inverted microscope. Data were collected using
140 with a Multiclamp 700B amplifier and Digidata 1550 data acquisition board (Molecular
141 Devices) using pClamp 10 software. During experiments in which both GABAergic and
142 glutamatergic autaptic PSCs were studied, the intracellular pipette solution consisted of
143 (in mM): 140 potassium chloride, 4 NaCl, 10 4-(2-hydroxyethyl)-1-

144 piperazineethanesulfonic acid (HEPES), 5 EGTA, and 0.5 CaCl₂. The pH was adjusted
145 to 7.25 with KOH. Experiments designed to examine excitatory postsynaptic currents
146 alone employed an internal solution containing 140 mM potassium gluconate instead of
147 potassium chloride to isolate glutamate-mediated currents. No exogenous ATP or
148 MgATP was added via the whole-cell pipette solution. Previous work on autaptic
149 hippocampal neurons has demonstrated that at least 10 min of recording time is required
150 for ~10% of the pipette contents to reach presynaptic terminals (Rosenmund and
151 Stevens, 1996). Therefore, whole-cell recordings obtained shortly after break-in should
152 rapidly establish postsynaptic ion gradients but effectively isolate presynaptic events
153 compromised by preceding metabolic manipulations.

154 Extracellular solution during voltage-clamp recordings typically consisted of (in
155 mM): 138 NaCl, 4 KCl, 10 HEPES, 10 glucose, 2 CaCl₂, 1 MgCl₂, and 0.01 D-2-amino-5-
156 phosphonovalerate (D-APV, Tocris), pH 7.25, adjusted with NaOH. Miniature PSCs and
157 experiments evoking vesicle release directly from synaptic terminals were recorded in
158 saline containing 1 μM TTX. For current clamp recordings, saline contained 2,3-Dioxo-
159 6-nitro-1,2,3,4-tetrahydrobenzo[*f*]quinoxaline-7-sulfonamide (NBQX, 1 μM) and
160 bicuculine (50 μM). All PSCs were autaptic, recorded from single-neuron microcultures,
161 except for mPSC analysis during metabolic inhibition in Figure 3, where recordings were
162 performed on cells in multi-neuron microcultures. This was done to ensure that the
163 majority of presynaptic events arose from cells whose metabolic state was not
164 influenced by the whole-cell recording pipette over the time periods required to monitor
165 mPSCs.

166 Whole-cell recording pipettes were pulled from borosilicate glass capillary tubes
167 (World Precision Instruments) and had final open-tip resistances 2-6 MΩ. Unless
168 otherwise stated, neurons in voltage-clamp mode were held at -70 mV. Evoked autaptic
169 PSCs were elicited with a 1.5 ms depolarizing pulse to 0 mV. Data were sampled at 20

170 kHz, filtered at 10 kHz for PSC recordings. Access resistance was compensated to 90%
171 for evoked autaptic PSC recordings. Miniature PSCs were sampled at 5 kHz and filtered
172 at 1 kHz; access resistance was not compensated. For recording action potentials in
173 current clamp mode, neurons were biased with small, tonic current injection when
174 necessary to hold the membrane potential near -65 mV. Depolarizing current pulses in
175 increments of 5-10 pA were applied for 1200 ms until a single action potential was
176 elicited. When solution exchange or drug delivery was performed, solutions were
177 dispensed to the target neuron by a gravity-driven local perfusion system from a
178 common tip with an exchange time of ~100 ms.

179

180 **Endocytosis measurement**

181 Fixable FM1-43 (FM1-43FX) dye labeling of vesicle cycling was performed as
182 previously detailed (Moulder et al., 2010). High density cell cultures were subjected
183 various metabolic conditions in the presence of 0.5 – 1 μ M TTX and 1 μ M NBQX, 25 μ M
184 D-APV for 20 min prior to probing for vesicle cycling with FM1-43FX. The probe was
185 conducted by challenging cells for 2 min with 5 μ M FM1-43FX (Thermo Fisher Scientific)
186 in 45 mM KCl to induce vesicle cycling. In the case of labeling in 0 Ca^{2+} solution, 100 μ M
187 EGTA was included to chelate residual Ca^{2+} during the probe. In other experiments
188 FM1-43FX was included during the 20 min metabolic challenge. In all cases, non-
189 internalized FM1-43FX fluorescence was removed with a brief application of saline
190 supplemented with 500 μ M Advasep-7 (CyDex). Cultures were washed 5 times with
191 saline then fixed for immunostaining with 4% paraformaldehyde and 0.2%
192 glutaraldehyde in PBS for 10 min at room temperature. Cultures were then washed with
193 PBS followed by a 10 minute incubation in 4% NGS and 0.04% Triton in PBS. Primary
194 antibody, anti-synapsin I (1:1000) was applied for 3 h at RT and washed twice in PBS
195 followed by 30 minute incubation in secondary antibody Alexa Fluor 633 conjugate

196 (Thermo Fisher Scientific), and glass coverslipping with Fluoromount G (Southern
197 Biotechnology Associates).

198 FM1-43FX and anti-synapsin I images were captured on an inverted Eclipse
199 TE2000-S microscope using a 60X objective with a 1.4 numerical aperture and a C1
200 scanning confocal laser (488, and 633 nm) with EZ-C1 software (Nikon). Z-stack images
201 were acquired with alternating laser lines while all gain and acquisition settings were
202 held constant within a given experiment. Two-dimensional projected images were
203 created and analyzed using Image J software and regions of interest to measure FM1-
204 43FX uptake/intensity were selected blindly using synapsin I-labeled puncta. FM1-43FX
205 fluorescence intensity was background subtracted, and puncta with intensity values
206 below background were assigned a value of 0.

207

208 **Data Analysis**

209 Data was analyzed and plotted using MetaMorph 7, Clampfit 10 (Molecular
210 Devices), MiniAnalysis 6 (Synaptosoft), Excel 2011 (Microsoft), Prism 6 (GraphPad), and
211 ImageJ. Unless otherwise stated, data in figures and text are given as mean \pm SEM.
212 Student's two-tailed unpaired *t* test was used to compare 2 groups unless otherwise
213 noted. If more than 2 parameters were compared between 2 groups, a Bonferroni
214 correction was applied. A One-Way ANOVA was used if comparing more than two
215 experimental conditions and a Two-way ANOVA was implemented when comparing the
216 effects of at least two parameters over time. To test differences in variance between
217 groups, an F-test was conducted. Non-parametric data were analyzed using a Kruskal-
218 Wallis one-way ANOVA followed by Dunn's multiple comparisons test. Significance was
219 defined as a corrected p-value < 0.05 . The reported n refers to the number of neurons
220 in each group within a particular experiment, except in imaging experiments where it

221 refers to the number of pre-synaptic terminals. In all cases at least 3 independent
222 cultures were surveyed, each contributing equally to final N values.

223

224 **Materials**

225 D-APV, NBQX, TTX, were obtained from Tocris Biosciences. All materials
226 without identified suppliers above were obtained from Sigma-Aldrich. 2-Deoxy-D-glucose
227 (2DG, 10 mM), oligomycin (oligo; 1 μ M), and alpha-cyano-4-hydroxycinnamic acid (4-
228 CIN, 100 μ M) are key pharmacological reagents used herein. 2DG and oligo are
229 commonly used at these concentrations to inhibit glycolysis and oxidative
230 phosphorylation, respectively (5-20 minutes; Schurr et al., 1999; Rangaraju et al., 2014;
231 Pathak et al., 2015; Lujan et al., 2016). At concentrations below 250 μ M, 4-CIN
232 effectively blocks lactate transport into neurons with very few off-target effects (Izumi et
233 al., 1997; Erlichman et al., 2008; Choi et al., 2012; Tang et al., 2014), although at higher
234 concentrations may have off-target effects (Chih et al., 2001). In our studies, an effect of
235 4-CIN was observed only when 4-CIN was combined with another metabolic
236 manipulation (2DG). This strongly suggests that 4-CIN at the concentration employed
237 acted through the intended mechanism.

238

239 **Results**

240 **Acute inhibition of both glycolysis and oxidative phosphorylation is required to** 241 **interfere with evoked synaptic transmission**

242 We initially tested the effect of acute inhibition of glycolysis and/or oxidative
243 phosphorylation on action potential-evoked synaptic transmission. Incubations in
244 metabolic poisons (2DG to inhibit glycolysis, oligo to inhibit oxidative phosphorylation, or
245 the combination) were performed 15 minutes prior to establishing whole-cell, patch-
246 clamp recordings from autaptic hippocampal neurons (Figure 1A). The whole-cell

247 recording configuration allowed direct control of postsynaptic ion gradients, so
248 presynaptic variables were effectively isolated by metabolic manipulations (see
249 Methods). Evoked postsynaptic currents (PSCs) were recorded immediately after break-
250 in and were typically measured for ~5 minutes at a 0.04 Hz stimulation frequency.
251 Inhibiting either glycolysis with 2DG (Figure 1B), or oxidative phosphorylation with an
252 ATP synthase inhibitor, oligo (Figure 1C), had no significant effect on the ability to evoke
253 PSCs in hippocampal neurons (Figure 1E). We observed no difference in effects on
254 glutamate- (N = 10, 7 cells, 2DG and oligo respectively) and GABA-mediated (N = 6, 10
255 cells, respectively) PSCs, so results were pooled. Average evoked PSC amplitude was
256 variable but did not differ among control (6.0 ± 0.7 nA, N = 19), oligo (4.3 ± 1.3 nA, N =
257 20), and 2DG conditions (6.8 ± 3.6 nA, N = 17). However, combined oligo and 2DG
258 (2DG+oligo) treatment significantly suppressed PSC amplitude (0.15 ± 0.02 nA, N = 16),
259 in most cases completely suppressing evoked PSCs (Figure 1D, E). PSCs were not
260 altered further during whole-cell recordings (5 min duration) in metabolic inhibitors; there
261 was no time-dependent decrement in PSCs with continued treatment with 2DG or oligo
262 alone (Figure 1F), and PSCs did not emerge during recording in the continued combined
263 presence of 2DG+oligo.

264 Interestingly, inhibition of oxidative phosphorylation alone or in the presence of
265 2DG was initially associated with suppressed axosomatic voltage-gated sodium currents
266 (Figure 1G,H), which drive presynaptic action potentials (Bekkers and Stevens, 1991;
267 Prakriya and Mennerick, 2000). This is in contrast to recent results at the calyx of Held,
268 where axonal action potentials were particularly sensitive to glycolytic inhibition (Lujan et
269 al., 2016). In our experiments the sodium currents in both oligo treatment groups grew
270 over time and were not significantly different from the glucose control group by 5 min
271 recording time, despite the lack of ATP in the pipette solution (Figure 1H). We posit that
272 the growth of sodium currents likely reflects the re-establishment of K^+ and Na^+ gradients

273 during cell dialysis with the patch pipette solution. We conclude that oxidative
274 phosphorylation is most important for maintaining these ion gradients and that glycolysis
275 alone is not sufficient.

276 To further characterize the effect of oligo on excitability, we examined somatic
277 action potentials in current-clamp recordings, using just-suprathreshold current injection
278 titrated for each cell. In this independent sample of neurons, both maximum rise rate and
279 peak amplitude of action potentials were depressed following 15 min of oligo incubation
280 compared with sibling control cells (Figure 1I). Despite initial suppression of sodium
281 currents in both oligo-treated groups (Figure 1H) and the effects of oligo on action
282 potential waveform (Figure 1I), transmission failure occurred only in neurons where both
283 glycolysis and oxidative phosphorylation were inhibited (Figure 1E). PSCs in this
284 condition did not recover despite the recovery of sodium current (Figure 1H). These
285 observations indirectly suggest that the disruption of sodium current alone is unlikely to
286 account for the depressed transmission when both glycolysis and oxidative
287 phosphorylation are inhibited.

288

289 **Inhibition of glycolysis and oxidative phosphorylation abolishes evoked vesicle**
290 **release.**

291 To test more directly whether action potential propagation deficits solely underlie
292 suppressed evoked PSCs, we challenged 2DG+oligo-treated cells with 100 mM K⁺
293 (substituted for Na⁺) in the presence of tetrodotoxin (TTX; 0.5-1 μ M) immediately
294 following the 15 minute incubation in saline with metabolic inhibitors or glucose control.
295 This evoked vesicle exocytosis through directly depolarization of terminals in the
296 absence of action potential firing (Prakriya and Mennerick, 2000). Direct depolarization
297 of unclamped presynaptic terminals elicited antagonist-sensitive PSCs in control
298 neurons (Figure 2A) but not in 2DG+oligo-treated cells (Figure 2B). Metabolically

299 poisoned neurons lost both the antagonist-sensitive peak (synchronous) release and
300 sustained release (Figure 2C,D).

301 Both action potentials and hyperkalemia require Ca^{2+} influx for exocytosis.
302 Depression of presynaptic Ca^{2+} influx following ATP loss could explain PSC loss. To by-
303 pass Ca^{2+} influx we utilized hypertonic sucrose, a Ca^{2+} independent secretagogue
304 (Rosenmund and Stevens, 1996). Sucrose (0.5 M) elicited antagonist-sensitive PSCs
305 from control neurons (Figure 2E, F, black trace) but not from 2DG+oligo-treated cells
306 (Figure 2E,F, blue trace). The loss of evoked release when action potentials and Ca^{2+}
307 influx are circumvented strongly suggests that neither action potential propagation nor
308 Ca^{2+} influx is the primary dysfunction underlying the loss of evoked PSCs after combined
309 inhibition glycolysis and oxidative phosphorylation. This outcome suggests that
310 releasable synaptic vesicles may be unavailable following metabolic inhibition.

311

312 **Metabolic poisoning fosters massive spontaneous vesicle release**

313 Although K^{+} - and sucrose-evoked vesicle release was completely abolished, we
314 were surprised that spontaneous miniature PSCs (mPSC) were still present in
315 2DG+oligo-treated cells (Figure 3B,C) and were comparable to mPSCs in controls
316 (Figure 3A). We found no significant difference in the mean frequency (Figure 3D),
317 amplitude (Figure 3E), 10-90% rise time (Figure 3F), or decay time (Figure 3G) between
318 control and 2DG+oligo-treated excitatory mPSCs (mEPSCs) and inhibitory mPSCs
319 (mIPSCs). These data suggest the presence of synaptic vesicles in the terminals, at
320 least initially, despite the inability to evoke release. On closer inspection of mPSCs, we
321 realized that metabolically compromised cells exhibited significantly greater variance in
322 mPSC frequency than control cells (Figure 3D; $F = 6.052$, $p < 0.0002$). We reasoned
323 that loss of ATP production may initiate vesicle release, and the large variance in
324 release frequency may correspond to different stages of metabolic poisoning in different

325 neurons.

326 We hypothesized that loss of presynaptic ATP induces massive spontaneous
327 vesicle exocytosis, which may contribute to the loss of evoked vesicle release. Thus,
328 neurons may experience increased mPSC frequency throughout incubation in the
329 metabolic poisons as presynaptic ATP levels are diminished; after 15 min incubation in
330 2DG+oligo neurons with a high mPSC frequency are still exocytosing, while cells with
331 low mPSC frequency have exhausted the ability to exocytose. Any exocytosis would be
332 independent of action potentials, as TTX was present during incubation of 2DG+oligo.

333 We directly tested whether loss of ATP affects vesicle fusion by recording
334 neurons throughout the 15 min incubation period in 2DG+oligo (Figure 3H-M) instead of
335 following the incubation period (Figure 3A-G). The protocol allowed us to observe
336 changes in mPSC frequency and evoked transmission within individual cells during
337 metabolic inhibition. We first evoked release in the presence of TTX with K^+ application
338 as in Figure 2A-D (Figure 3H,I black traces) and then measured mPSC frequency in the
339 presence of either glucose control or metabolic inhibitors over the course of 15 min.
340 Following 15 min of glucose (control) or 2DG+oligo treatment, we re-assessed evoked
341 PSCs. PSCs were mildly depressed in control cells, but were abolished in the
342 2DG+oligo treatment (Figure 3H-J). In the same cells, mPSC frequency was initially high
343 following the initial K^+ challenge, reflecting residual presynaptic Ca^{2+} (Figure 3K, L). In
344 control neurons, mPSC frequency immediately subsided, but in 2DG+oligo cells, the
345 mPSC frequency remained elevated before decreasing to near-control levels by 15 min
346 (Figure 3K-M).

347 In a separate experiment mPSC frequency was quantified over the 15 min
348 incubation in either 2DG+oligo or glucose controls without the accompanying K^+ -evoked
349 PSC challenge. We once again observed a significant increase in mPSC frequency in
350 the presence of 2DG+oligo compared to glucose controls (Figure 3N-P). Thus, the large

351 initial mPSC frequency elicited by K^+ in Figure 3H-M was not necessary to initiate the
352 sustained elevation of mPSC frequency in metabolically poisoned cells. These
353 observations suggest that tandem inhibition of glycolysis and oxidative phosphorylation
354 produces massive synaptic exocytosis. Although some degree of spontaneous release
355 still persists following 15 min of poisoning, evoked release is nearly abolished.

356

357 **Endocytic failure after metabolic poisoning**

358 Because vesicles are recycled, mass exocytosis alone would not account for the
359 loss of evoked vesicle release following incubation in 2DG+oligo. Recent work has
360 shown that ATP levels also influence vesicle endocytosis, with glycolysis playing a
361 particularly important role (Rangaraju et al., 2014; Pathak et al., 2015; Jang et al., 2016).
362 To test whether endocytosis was arrested in metabolically poisoned neurons, we
363 measured vesicle cycling with FM1-43FX to label vesicle internalization at presynaptic
364 terminals, identified with synapsin I (Figure 4A). Cultures were incubated for 20 minutes
365 in the indicated conditions. Following incubation, vesicle cycling was probed by adding
366 FM1-43FX and 45 mM K^+ for 2 min. Neither 2DG (Figure 4C,G burgundy bar) nor oligo
367 (Figure 4,D,G teal bar) altered vesicle cycling, but co-administration of 2DG+oligo
368 significantly reduced vesicle cycling during the probe period (Figure 4E,G blue bar).

369 To confirm that diminished cycling resulted from metabolic poisoning and not
370 from prolonged vesicle exocytosis, we simulated the extended exocytosis observed in
371 2DG+oligo-treated cells using 45 mM K^+ (substituted for Na^+) present for 20 min with
372 TTX but without any metabolic inhibition. Exposure to 45 mM K^+ produced a similar
373 steady-state mPSC frequency compared with 2DG+oligo treatment (25.74 ± 11.72 Hz, n
374 = 5 K^+ -challenged cells), but vesicle cycling during a subsequent 2 min probe in FM1-
375 43FX was not significantly affected (Figure 4B,G orange bar). Finally, we measured
376 FM1-43FX labeling in a control group lacking Ca^{2+} in the probe condition to diminish

377 vesicle cycling during FM1-43FX loading. Cycling was significantly reduced (Figure 4F,G
378 gray bar), comparable to when neurons were metabolically poisoned. This control
379 condition also confirms the synaptic nature of labeling.

380 Experiments in Figure 4 confirm that vesicle cycling, rather than vesicle filling or
381 other potential explanations, is associated with the loss of evoked transmission during
382 combined 2DG+oligo treatment. However, the experiments do not specifically determine
383 whether arrested endocytosis contributes. To test this, we incubated cells in FM1-43FX
384 throughout the entire 20 min period of poisoning, during which massive exocytosis
385 occurs (Figure 3M). As a control, we again depolarized cells in the presence of TTX to
386 produce a comparably stimulated rate of exocytosis, but without metabolic inhibition. The
387 net FM1-43FX labeling during the 20 min incubation in 2DG+oligo (Figure 5A-B, blue
388 bar) was no different than control (Figure 5A-B, black bar), while K^+ stimulation produced
389 the FM1-43FX labeling expected of ongoing vesicle cycling (Figure 5A-B, orange bar).
390 The lack of staining in the unstimulated control (Figure 5A, left panel; Figure 5B, black
391 bar) presumably reflects the low rate of mPSCs per synapse in the 15 min incubation.
392 Overall, the results demonstrate that the massive exocytosis during metabolic inhibition
393 is not followed by compensatory endocytosis. Thus, arrested endocytosis likely explains
394 the loss of evoked vesicle release. The results demonstrate an important role for
395 continuous ATP production, flexibly driven by either glycolysis or oxidative
396 phosphorylation, in synaptic vesicle cycling.

397

398 **Oxidative phosphorylation powers recovery following intense presynaptic**
399 **transmission.**

400 Although either glycolysis or oxidative phosphorylation proved capable of
401 sustaining basal transmission (Figure 1), we wondered if a more energetically
402 demanding stimulus would reveal a privileged role for presynaptic glycolysis or oxidative

403 phosphorylation. We examined the recovery of excitatory PSCs (EPSCs) after a brief,
404 strong depolarization designed to empty all recycling vesicles (Sara et al., 2002; Chung
405 et al., 2010). Glutamate synaptic signaling and uptake may be more energetically
406 demanding than GABA signaling (Waldvogel et al., 2000; Chatton et al., 2003), so we
407 focused on EPSCs. As schematized in Figure 6A, we measured baseline evoked
408 EPSCs, applied 90mM K⁺ for 30s to deplete the vesicle pool, and then measured the
409 recovery of EPSCs with action potential stimulation every 25 s for ~2 min.

410 2DG incubation did not significantly affect EPSC recovery after vesicle depletion
411 compared to glucose-incubated controls (Figure 6B,D). However, oligo alone
412 significantly diminished recovery (Figure 6C,E). Slower recovery did not result from
413 action potential deficits because sodium action currents remained at pre-challenge levels
414 for both oligo treated cells and control cells (Figure 6G). These data suggest that
415 glycolysis alone cannot adequately sustain presynaptic recovery following a high-
416 demand stimulus. Rather, oxidative phosphorylation, perhaps because of its larger ATP
417 yield, has a privileged role in fueling recovery of presynaptic function after vesicle
418 depletion. Further, the lack of a 2DG effect implies that on-demand glycolysis is not
419 necessary to supply pyruvate for oxidative phosphorylation during the challenge. This
420 suggests that neurons power presynaptic function with reserve or alternative substrates
421 for oxidative phosphorylation when glycolysis is inhibited.

422

423 **Endogenous monocarboxylate powers oxidative phosphorylation when glycolysis**
424 **is inhibited**

425 Attractive candidates for alternative metabolic substrates during glycolytic
426 inhibition include monocarboxylates, such as lactate (Schurr et al., 1988; Izumi et al.,
427 1997; Ivanov et al., 2011; Wyss et al., 2011). Extracellular recording solutions do not
428 contain exogenous monocarboxylates, so based on prevailing views lactate would be

429 shuttled on demand from astrocytes to neurons during increased glutamate signaling
430 (e.g., following vesicle depletion) to supply the TCA cycle with pyruvate (Pellerin and
431 Magistretti, 1994, 2012). Microcultures provide a unique opportunity to test local
432 shuttling, and we tested the local shuttle hypothesis by culturing neurons in the absence
433 of contact with an astrocyte bed (Sobieski et al., 2015). We previously showed that
434 neurons without astrocyte contact exhibit altered synchrony of evoked glutamate release
435 (-astrocyte; Figure 7B) compared to astrocyte-supported controls (+astrocyte; Figure
436 7A), but many other facets of evoked transmission are intact (Sobieski et al., 2015).
437 Recovery of EPSCs following the vesicle depletion challenge was slightly depressed in -
438 astrocyte neurons compared with +astrocyte neurons when recorded in control medium
439 (Figure 7C), but this effect was not statistically significant. Furthermore,
440 incubation/recording in saline with lactate (1.5 mM) in place of glucose did not increase
441 EPSC recovery after vesicle depletion (Figure 7D). Therefore, any deficit in the recovery
442 of -astrocyte EPSCs cannot be accounted for by the loss of astrocyte-derived lactate.

443 Although these observations exclude a strong role for local, on-demand
444 monocarboxylate shuttling as envisioned by the astrocyte-neuron lactate shuttle
445 hypothesis (Pellerin and Magistretti, 1994, 2012), it is possible that bulk lactate levels
446 derived from the summed contributions of surrounding astrocytes participates in fueling
447 recovery from vesicle depletion. We tested the importance of global lactate efflux by
448 pharmacologically inhibiting monocarboxylate transport with the monocarboxylate
449 transport inhibitor 4-CIN, 100 μ M for 15 min. 4-CIN had no effect on EPSC recovery after
450 total vesicle depletion (Figure 8A,C). These results suggest that either neuronal
451 glycolysis or perhaps the breakdown of alternative fuel reserves can support synaptic
452 transmission when lactate shuttling alone is inhibited.

453 Reducing either neuronal glycolysis (Figure 6D) or monocarboxylate transport
454 (Figure 8C) to diminish supply of substrates to the TCA cycle yielded little effect on

455 EPSC recovery after vesicle depletion. These data suggest two sources of fuel for
456 oxidative phosphorylation, either of which can support EPSC recovery following
457 depletion. We next examined the combined effects of inhibition of monocarboxylate
458 transport and glycolysis. Co-administration of 2DG and 4-CIN significantly reduced
459 EPSC recovery after vesicle depletion (Figure 8B,D). Thus, although inhibition of neither
460 monocarboxylate transport (Figure 8A,C) nor neuronal glycolysis alone (Figure 6B,D)
461 altered recovery, combined inhibition of both partially arrested EPSC recovery,
462 equivalent to the effect of oligo (Figure 6C,E). These data suggest that oxidative
463 phosphorylation continuously supplies ATP necessary for synaptic vesicle recovery after
464 depletion, and substrate for oxidative phosphorylation can originate from either
465 extracellular monocarboxylates or from neuronal glycolysis.

466

467 **Discussion**

468 In this study, we investigated the sources of ATP synthesis that drive basal
469 presynaptic function and recovery of function following high energetic demand. Our work
470 shows that ongoing ATP production, either through glycolysis or oxidative
471 phosphorylation, sustains evoked synaptic transmission for up to 20 min. Only the
472 combined inhibition of glycolysis and oxidative phosphorylation abolished PSCs evoked
473 at low frequency. The loss of evoked transmission likely results from massive
474 spontaneous vesicle release and subsequent failure to endocytose vesicles. Our data
475 also suggest that oxidative phosphorylation has a privileged role in powering the rapid
476 recovery of EPSCs after vesicle depletion. Neuronal presynaptic oxidative
477 phosphorylation appears to be flexible in use of energetic substrates, as either neuronal
478 glycolysis or astrocyte-derived monocarboxylates sufficed to fuel recovery. Overall, our
479 work elucidates the sources of presynaptic ATP during basal and high-demand activity.

480 Our work adds mechanistic details to previous studies that have highlighted the
481 energetic demand of neurons in brain slices. Excitatory postsynaptic potentials in
482 hippocampal slices are very sensitive to glucose deprivation (Schurr et al., 1988; Izumi
483 et al., 1994, 1997). However, the roles of presynaptic and postsynaptic factors and of
484 glycolysis versus oxidative phosphorylation have been unclear. In slices, energetic
485 depression leads to accumulation of neurotransmitters and other secondary changes. It
486 can be difficult to know whether changes to transmission are a direct consequence of
487 changes to ATP levels or to these secondary consequences. Further, the trauma of
488 tissue preparation can cause important metabolic changes that affect results (Takano et
489 al., 2014). Although cultures have their own limitations, they allow experimental control
490 not possible *in situ*, including our isolation of local versus global astrocyte contributions.

491 Several of our observations appear to conflict with other recent studies. Figure
492 1H suggests that ion gradients are rapidly compromised by inhibition of ATP produced
493 by oxidative phosphorylation. Other recent work found that the Na^+/K^+ ATPase is a
494 relatively light burden on presynaptic ATP levels (Rangaraju et al., 2014). One
495 reconciliation could be that ATP demands are compartmentalized, with more ATPase
496 burden near the soma, where our whole-cell recordings of sodium currents and action
497 potentials were made. However, another complication is that at the calyx of Held
498 synapse, presynaptic axonal action potential waveform is quite sensitive to glycolytic
499 inhibition due to collapse of ion gradients (Lujan et al., 2016). There are two surprising
500 things about these results compared with ours. First, we found that inhibition of oxidative
501 phosphorylation alone, rather than glycolysis alone, produced changes to sodium current
502 and action potential waveform. Second, because hippocampal glutamate release is
503 quite sensitive to changes in action potential waveform (Prakriya and Mennerick, 2000;
504 Meeks and Mennerick, 2004; Sobieski et al., 2015; Lujan et al., 2016), if the somatic
505 action potential waveform changes we observed following oligo treatment alone were

506 propagated to terminals, we would have expected strong alteration of transmitter
507 release. Instead, we found that the changes to excitability produced by oligo alone were
508 not associated with deficits in evoked PSCs.

509 Our results also differ from others with regard to the role of glycolysis on
510 endocytosis. Previous work suggests that endocytosis relies heavily on glycolysis
511 (Rangaraju et al., 2014; Pathak et al., 2015). In contrast, we observed that vesicle
512 endocytosis, measured by FM1-43FX fluorescence (Figure 4C, G burgundy bar), and
513 PSCs recovered well following sole inhibition of glycolysis (Figure 6D). The reasons for
514 the discrepancies are unclear, but could relate to use of different methods to measure
515 presynaptic activity.

516 Our observations uncovered massive vesicle exocytosis during combined
517 glycolytic and oxidative phosphorylation inhibition. Similar effects have been observed
518 following oxygen-glucose deprivation (Allen et al., 2004; Fujimoto et al., 2004) or
519 pharmacological manipulation of glycolysis and oxidative phosphorylation (Lujan et al.,
520 2016). Endocytic failure following the mass vesicle exocytosis appears sufficient to
521 explain the loss of evoked PSCs (Figure 5); however, we cannot exclude other
522 contributing mechanisms, such as ATP-dependent vesicle filling or vesicle priming, to
523 the loss of evoked PSCs. The precise cause of the massive exocytosis remains unclear.
524 Collapse of ion gradients and consequent depolarization-dependent calcium influx or
525 mitochondrial efflux could participate (Lujan et al., 2016). Other Ca^{2+} -independent
526 possibilities include electrostatic effects of ATP on synaptotagmin-1 function and ATP
527 dependent SNARE complex disassembly (Park et al., 2012).

528 The persistence of spontaneous mPSCs following metabolic inhibition could
529 suggest differential sensitivity of vesicle pools underlying spontaneous and evoked
530 neurotransmission (reviewed in Crawford and Kavalali, 2015). It is tempting to speculate
531 that the different molecular identities of the two pools afford them different energetic

532 sensitivity, or that ATP depletion shifts the evoked pool of vesicles into a spontaneous-
533 only mode of release. Alternatively, the residual mPSCs during the period of abolished
534 evoked transmission could simply reflect a few remaining functional terminals that were
535 not readily detected in our measures of evoked release. In the future it will be important
536 to explore the differential neuroenergetics of spontaneous and evoked release in more
537 detail.

538 An important conclusion from our work is that oxidative phosphorylation plays a
539 more prominent role than glycolysis in fueling recovery of transmission following brief,
540 intense metabolic challenge. Vesicle endocytosis, as probed by FM1-43FX uptake
541 (Figure 4D, G teal bar), was unperturbed by pre-treatment with oligo. This suggests that
542 the depression of recovery of evoked EPSCs following depolarizing challenge (Figure
543 6C, E) likely results from a mechanism other than endocytic arrest, such as a deficit in
544 replenishment of vesicles from the reserve pool or vesicle filling.

545 The importance of oxidative phosphorylation for EPSC recovery after a strong
546 presynaptic stimulus could implicate the astrocyte-neuron lactate shuttle (Pellerin and
547 Magistretti, 1994; Takahashi et al., 1995; Bittner et al., 2010). However, neither
548 pharmacological inhibition of monocarboxylate transport (Figure 8A,C) nor removal of
549 local astrocyte support (Figure 7A-C) altered EPSC recovery. Thus, local, on-demand
550 lactate shuttling from astrocytes in response to increased activity does not account for
551 presynaptic recovery. In fact, EPSC recovery after vesicle depletion was only reduced by
552 obstructing both glycolysis and monocarboxylate transport to neurons (Figure 8B,D),
553 effectively cutting off two main fuel supplies for oxidative phosphorylation. These findings
554 suggest that oxidative phosphorylation fueling presynaptic recovery can be effectively
555 sourced by either neuronal glycolysis or by ambient, global monocarboxylates.

556 Interestingly, basal synaptic transmission was not ablated with co-incubation of
557 2DG and 4-CIN as it was with 2DG and oligo (Figure 1D,E). The inability of combined

558 2DG/4-CIN to depress basal evoked synaptic transmission most likely results from
559 incomplete inhibition of monocarboxylate transport by 4-CIN. Alternatively, additional
560 substrates for oxidative phosphorylation could maintain basal function. One alternative is
561 glutamate, which can be converted to alpha-ketoglutarate, an important TCA
562 intermediate and potential source of pyruvate (McKenna, 2007). Ketone bodies
563 represent another alternative fuel and direct source for acetyl-Co-A (Izumi et al., 1998).
564 Typically ketone bodies are derived peripherally, with questionable relevance to
565 dissociated cultures, but they also may be produced by astrocytes (Takahashi et al.,
566 2014). In future work, it would be intriguing to query to roles of these fuel sources in
567 fueling synaptic transmission and presynaptic function.

568 The relative importance of oxidative phosphorylation over glycolysis is also
569 interesting because of the presynaptic compartmentalization of glycolysis and oxidative
570 phosphorylation within the neuron. Early and more recent work have found that glycolytic
571 machinery in the presynaptic cytosol maintains K^+ homeostasis by fueling Na^+/K^+ -
572 ATPase activity (Knull, 1978; Lipton and Whittingham, 1982; Lujan et al., 2016).
573 Mitochondria, on the other hand, reside in only 25-40% of presynaptic terminals (Chavan
574 et al., 2015; Pathak et al., 2015). Despite the sporadic localization of mitochondria to
575 presynaptic terminals, our work as well as others demonstrate that oxidative
576 phosphorylation is important for presynaptic function (Verstreken et al., 2005; Kang et
577 al., 2008; Hall et al., 2012; Sun et al., 2013; Pathak et al., 2015). Thus, sparse
578 mitochondria apparently produce sufficient ATP to supply neighboring boutons (Pathak
579 et al., 2015).

580 In conclusion, synaptic transmission is surprisingly resilient to changes in
581 metabolic substrate availability. Either glycolysis or oxidative phosphorylation suffices to
582 fuel basal synaptic transmission, but loss of both leads to a massive release of synaptic
583 vesicles, diminished vesicle endocytosis, and evoked PSC loss. Further metabolic

584 challenges, such as strong depolarization, reveal a preferential role of oxidative
585 phosphorylation in producing the ATP required for presynaptic recovery. In turn oxidative
586 phosphorylation is fueled by either neuronal glycolysis or by transport of ambient
587 monocarboxylates, likely from astrocytes. Impeding both fuel supplies weakens EPSC
588 recovery. Taken together, our data showcase the flexibility of neurons to changes in
589 metabolic substrate availability in order to maintain presynaptic function.
590

591 **References**

- 592 Allen NJ, Rossi DJ, Attwell D (2004) Sequential release of GABA by exocytosis and
593 reversed uptake leads to neuronal swelling in simulated ischemia of hippocampal
594 slices. *J Neurosci* 24:3837–3849.
- 595 Attwell D, Laughlin SB (2001) An energy budget for signaling in the grey matter of the
596 brain. *J Cereb Blood Flow Metab* 21:1133–1145.
- 597 Auestad N, Korsak RA, Morrow JW, Edmond J (1991) Fatty acid oxidation and
598 ketogenesis by astrocytes in primary culture. *J Neurochem* 56:1376–1386.
- 599 Bekkers JM, Stevens CF (1991) Excitatory and inhibitory autaptic currents in isolated
600 hippocampal neurons maintained in cell culture. *Proc Natl Acad Sci U S A* 88:7834–
601 7838.
- 602 Bittner CX, Loaiza A, Ruminot I, Larenas V, Sotelo-Hitschfeld T, Gutiérrez R, Córdova A,
603 Valdebenito R, Frommer WB, Barros LF (2010) High resolution measurement of the
604 glycolytic rate. *Front Neuroenergetics* 2.
- 605 Chatton J-Y, Pellerin L, Magistretti PJ (2003) GABA uptake into astrocytes is not
606 associated with significant metabolic cost: implications for brain imaging of
607 inhibitory transmission. *Proc Natl Acad Sci U S A* 100:12456–12461.
- 608 Chavan V, Willis J, Walker SK, Clark HR, Liu X, Fox MA, Srivastava S, Mukherjee K
609 (2015) Central presynaptic terminals are enriched in ATP but the majority lack
610 mitochondria. *PLoS One* 10:e0125185.
- 611 Chih C-P, He J, Sly TS, Roberts EL (2001) Comparison of glucose and lactate as
612 substrates during NMDA-induced activation of hippocampal slices. *Brain Res*
613 893:143–154.
- 614 Choi HB, Gordon GRJ, Zhou N, Tai C, Rungta RL, Martinez J, Milner TA, Ryu JK,
615 McLarnon JG, Tresguerres M, Levin LR, Buck J, MacVicar BA (2012) Metabolic
616 communication between astrocytes and neurons via bicarbonate-responsive

- 617 soluble adenylyl cyclase. *Neuron* 75:1094–1104.
- 618 Chung C, Barylko B, Leitz J, Liu X, Kavalali ET (2010) Acute dynamin inhibition dissects
619 synaptic vesicle recycling pathways that drive spontaneous and evoked
620 neurotransmission. *J Neurosci* 30:1363–1376.
- 621 Crawford DC, Jiang X, Taylor A, Mennerick S (2012) Astrocyte-derived thrombospondins
622 mediate the development of hippocampal presynaptic plasticity in vitro. *J Neurosci*
623 32:13100–13110.
- 624 Crawford DC, Kavalali ET (2015) Molecular underpinnings of synaptic vesicle pool
625 heterogeneity. *Traffic* 16:338–364.
- 626 Edmond J, Robbins RA, Bergstrom JD, Cole RA, de Vellis J (1987) Capacity for
627 substrate utilization in oxidative metabolism by neurons, astrocytes, and
628 oligodendrocytes from developing brain in primary culture. *J Neurosci Res* 18:551–
629 561.
- 630 Erlichman JS, Hewitt A, Damon TL, Hart M, Kuraszcz J, Li A, Leiter JC (2008) Inhibition
631 of monocarboxylate transporter 2 in the retrotrapezoid nucleus in rats: a test of the
632 astrocyte-neuron lactate-shuttle hypothesis. *J Neurosci* 28:4888–4896.
- 633 Fujimoto S, Katsuki H, Kume T, Kaneko S, Akaike A (2004) Mechanisms of oxygen
634 glucose deprivation-induced glutamate release from cerebrocortical slice cultures.
635 *Neurosci Res* 50:179–187.
- 636 Gallagher CN et al. (2009) The human brain utilizes lactate via the tricarboxylic acid
637 cycle: a ¹³C-labelled microdialysis and high-resolution nuclear magnetic resonance
638 study. *Brain* 132:2839–2849.
- 639 Hall CN, Klein-Flugge MC, Howarth C, Attwell D (2012) Oxidative phosphorylation, not
640 glycolysis, powers presynaptic and postsynaptic mechanisms underlying brain
641 information processing. *J Neurosci* 32:8940–8951.
- 642 Harris JJ, Jolivet R, Attwell D (2012) Synaptic energy use and supply. *Neuron* 75:762–

- 643 777.
- 644 Hertz L, Drejer J, Schousboe A (1988) Energy metabolism in glutamatergic neurons,
645 GABAergic neurons and astrocytes in primary cultures. *Neurochem Res* 13:605–
646 610.
- 647 Ikemoto A, Bole DG, Ueda T (2003) Glycolysis and glutamate accumulation into synaptic
648 vesicles. Role of glyceraldehyde phosphate dehydrogenase and 3-
649 phosphoglycerate kinase. *J Biol Chem* 278:5929–5940.
- 650 Ivanov A, Mukhtarov M, Bregestovski P, Zilberter Y (2011) Lactate effectively covers
651 energy demands during neuronal network activity in neonatal hippocampal slices.
652 *Front Neuroenergetics* 3:2.
- 653 Izumi Y, Benz AM, Katsuki H, Zorumski CF (1997) Endogenous monocarboxylates
654 sustain hippocampal synaptic function and morphological integrity during energy
655 deprivation. *J Neurosci* 17:9448–9457.
- 656 Izumi Y, Benz AM, Zorumski CF, Olney JW (1994) Effects of lactate and pyruvate on
657 glucose deprivation in rat hippocampal slices. *Neuroreport* 5:617–620.
- 658 Izumi Y, Ishii K, Katsuki H, Benz AM, Zorumski CF (1998) beta-Hydroxybutyrate fuels
659 synaptic function during development. Histological and physiological evidence in rat
660 hippocampal slices. *J Clin Invest* 101:1121–1132.
- 661 Jang S, Nelson JC, Bend EG, Rodríguez-Laureano L, Tueros FG, Cartagena L,
662 Underwood K, Jorgensen EM, Colón-Ramos DA (2016) Glycolytic enzymes localize
663 to synapses under energy stress to support synaptic function. *Neuron* 90:278–291.
- 664 Kang J-S, Tian J-H, Pan P-Y, Zald P, Li C, Deng C, Sheng Z-H (2008) Docking of
665 Axonal Mitochondria by Syntaphilin Controls Their Mobility and Affects Short-Term
666 Facilitation. *Cell* 132:137–148.
- 667 Knull HR (1978) Association of glycolytic enzymes with particulate fractions from nerve
668 endings. *Biochim Biophys Acta* 522:1–9.

- 669 Lipton P, Whittingham TS (1982) Reduced ATP concentration as a basis for synaptic
670 transmission failure during hypoxia in the in vitro guinea-pig hippocampus. *J Physiol*
671 325:51–65.
- 672 Lujan B, Kushmerick C, Das Banerjee T, Dagda RK, Renden R (2016) Glycolysis
673 selectively shapes the presynaptic action potential waveform. *J Neurophysiol*. In
674 Press.
- 675 McKenna MC (2007) The glutamate-glutamine cycle is not stoichiometric: Fates of
676 glutamate in brain. *J Neurosci Res* 85:3347–3358.
- 677 McKenna MC (2012) Substrate competition studies demonstrate oxidative metabolism of
678 glucose, glutamate, glutamine, lactate and 3-hydroxybutyrate in cortical astrocytes
679 from rat brain. *Neurochem Res* 37:2613–2626.
- 680 Meeks JP, Mennerick S (2004) Selective effects of potassium elevations on glutamate
681 signaling and action potential conduction in hippocampus. *J Neurosci* 24:197–206.
- 682 Mennerick S, Zorumski CF (1995) Paired-pulse modulation of fast excitatory synaptic
683 currents in microcultures of rat hippocampal neurons. *J Physiol* 488:85–101.
- 684 Moulder KL, Jiang X, Taylor AA, Benz AM, Mennerick S (2010) Presynaptically Silent
685 Synapses Studied with Light Microscopy. *J Vis Exp*:e1676–e1676.
- 686 Moulder KL, Jiang X, Taylor AA, Shin W, Gillis KD, Mennerick S (2007) Vesicle pool
687 heterogeneity at hippocampal glutamate and GABA synapses. *J Neurosci* 27:9846–
688 9854.
- 689 Park Y, Hernandez JM, van den Bogaart G, Ahmed S, Holt M, Riedel D, Jahn R (2012)
690 Controlling synaptotagmin activity by electrostatic screening. *Nat Struct Mol Biol*
691 19:991–997.
- 692 Pathak D, Shields LY, Mendelsohn BA, Haddad D, Lin W, Gerencser AA, Kim H, Brand
693 MD, Edwards RH, Nakamura K (2015) The role of mitochondrially derived ATP in
694 synaptic vesicle recycling. *J Biol Chem* 290:22325–22336.

- 695 Pellerin L, Magistretti PJ (1994) Glutamate uptake into astrocytes stimulates aerobic
696 glycolysis: a mechanism coupling neuronal activity to glucose utilization. *Proc Natl*
697 *Acad Sci U S A* 91:10625–10629.
- 698 Pellerin L, Magistretti PJ (2012) Sweet sixteen for ANLS. *J Cereb Blood Flow Metab*
699 32:1152–1166.
- 700 Pfeiffer T et al. (2001) Cooperation and competition in the evolution of ATP-producing
701 pathways. *Science* 292:504–507.
- 702 Prakriya M, Mennerick S (2000) Selective depression of low-release probability
703 excitatory synapses by sodium channel blockers. *Neuron* 26:671–682.
- 704 Rangaraju V, Calloway N, Ryan TA (2014) Activity-driven local ATP synthesis is required
705 for synaptic function. *Cell* 156:825–835.
- 706 Rosenmund C, Stevens CF (1996) Definition of the readily releasable pool of vesicles at
707 hippocampal synapses. *Neuron* 16:1197–1207.
- 708 Sara Y, Mozhayeva MG, Liu X, Kavalali ET (2002) Fast vesicle recycling supports
709 neurotransmission during sustained stimulation at hippocampal synapses. *J*
710 *Neurosci* 22:1608–1617.
- 711 Schurr A, Miller JJ, Payne RS, Rigor BM (1999) An increase in lactate output by brain
712 tissue serves to meet the energy needs of glutamate-activated neurons. *J Neurosci*
713 19:34–39.
- 714 Schurr A, West CA, Rigor BM (1988) Lactate-supported synaptic function in the rat
715 hippocampal slice preparation. *Science* 240:1326–1328.
- 716 Sobieski C, Jiang X, Crawford DC, Mennerick S (2015) Loss of local astrocyte support
717 disrupts action potential propagation and glutamate release synchrony from
718 unmyelinated hippocampal axon terminals in vitro. *J Neurosci* 35:11105–11117.
- 719 Sonnewald U, White LR, Ødegård E, Westergaard N, Bakken IJ, Aasly J, Unsgård G,
720 Schousboe A (1996) MRS study of glutamate metabolism in cultured neurons/glia.

- 721 Neurochem Res 21:987–993.
- 722 Sun T, Qiao H, Pan P-Y, Chen Y, Sheng Z-H (2013) Motile axonal mitochondria
723 contribute to the variability of presynaptic strength. *Cell Rep* 4:413–419.
- 724 Takahashi S, Driscoll BF, Law MJ, Sokoloff L (1995) Role of sodium and potassium ions
725 in regulation of glucose metabolism in cultured astroglia. *Proc Natl Acad Sci U S A*
726 92:4616–4620.
- 727 Takahashi S, Iizumi T, Mashima K, Abe T, Suzuki N (2014) Roles and regulation of
728 ketogenesis in cultured astroglia and neurons under hypoxia and hypoglycemia.
729 *ASN Neuro* 6.
- 730 Takano T, He W, Han X, Wang F, Xu Q, Wang X, Oberheim Bush NA, Cruz N, Dienel
731 GA, Nedergaard M (2014) Rapid manifestation of reactive astrogliosis in acute
732 hippocampal brain slices. *Glia* 62:78–95.
- 733 Tang F et al. (2014) Lactate-mediated glia-neuronal signalling in the mammalian brain.
734 *Nat Commun* 5:ra26.
- 735 Verstreken P, Ly C V, Venken KJT, Koh T-W, Zhou Y, Bellen HJ (2005) Synaptic
736 mitochondria are critical for mobilization of reserve pool vesicles at *Drosophila*
737 neuromuscular junctions. *Neuron* 47:365–378.
- 738 Waldvogel D, van Gelderen P, Muellbacher W, Ziemann U, Immisch I, Hallett M (2000)
739 The relative metabolic demand of inhibition and excitation. *Nature* 406:995–998.
- 740 Wyss MT, Jolivet R, Buck A, Magistretti PJ, Weber B (2011) In vivo evidence for lactate
741 as a neuronal energy source. *J Neurosci* 31:7477–7485.
- 742
- 743

744 **Figure Legends.**
745

746 **Figure 1.** Acute inhibition of glycolysis and oxidative phosphorylation impairs evoked
747 vesicle release. **A-D.** Representative evoked autaptic EPSCs elicited in each of the
748 indicated conditions, after 15 min pre-incubation in the conditions prior to establishing
749 the whole-cell recording. '2DG' designates substitution of 2DG (10 mM) for glucose.
750 Oligo was applied at 1 μ M. The dashed boxes indicate presynaptic stimulation currents,
751 including an inward sodium current highlighted in panel G. **E.** Neurons exhibiting PSCs
752 or no detectable PSC, from the four conditions, color-coded according to the text labels
753 in A-D (n = 16-20 neurons per condition). 2DG+oligo exhibited significantly more
754 neurons lacking evoked PSCs than control glucose (chi-square, $X^2 = 30.35$, $p < 0.0001$).
755 **F.** Summary of evoked PSCs obtained following 5 min stimulation (0.04 Hz), normalized
756 to initial currents obtained on membrane break-in. There was no significant difference in
757 PSC peak size of glucose, 2DG, or oligo alone after 5 min of recording compared to
758 immediate break-in ($p > 0.05$ for all conditions; two-way repeated measures ANOVA with
759 Bonferroni corrections performed on raw data). No PSCs were evident at time 0 or 5 min
760 after break-in in the 2DG+oligo condition, hence the lack of bar. **G.** Representative
761 sodium currents measured immediately on break-in in the four experimental conditions
762 taken from the time period indicated by the dashed boxes in A-D. Colors correspond to
763 the text labels in A-D. **H.** Summary of sodium current obtained immediately after break-in
764 and after 5 min of stimulation, normalized to 0 min glucose sodium current. At 0 min, the
765 oligo and 2DG+oligo conditions were significantly smaller than glucose controls ($p <$
766 0.01 , 0.0001 for oligo and 2DG+oligo, respectively; two-way repeated measures ANOVA
767 with Bonferroni corrections performed on raw data) At 5 min there was no significant
768 difference between glucose and the three remaining conditions ($p > 0.05$ for all
769 conditions, two-way repeated measures ANOVA with Bonferroni corrections performed

770 on raw data). Data are represented as mean \pm SEM. ** $p \leq 0.01$. *** $p \leq 0.001$. n.s, non-
771 significant. **I.** Action potential waveform changes resulting from oligo-only treatment.
772 Current-clamp recordings were established after incubations as above, and a family of
773 depolarizing currents (5-10 pA increment, 1200 ms) was injected to elicit a just-
774 suprathreshold action potential. Peak and maximum rate of rise were measured in 27
775 control neurons and 25 oligo-treated neurons. The inset shows an exemplar action
776 potential from one cell in each condition superimposed.

777

778 **Figure 2.** Presynaptic vesicle release is also impaired when action potentials and
779 calcium influx are by-passed. **A,B.** Representative autaptic currents evoked by 100 mM
780 K^+ for 3 s, as indicated by the horizontal bar. Red traces indicate the same treatment,
781 but in the presence of a cocktail of postsynaptic receptor blockers (1 μ M NBQX, 50 μ M
782 bicuculline), revealing non-synaptic currents elicited by K^+ . **C,D.** Summary of
783 antagonist-sensitive peak PSC amplitude and total charge transfer for the two conditions
784 ($n=12,12$; $p < 0.001, 0.01$, respectively, unpaired, two-tailed Student's t -test with
785 Bonferroni corrections) measured from the antagonist-subtracted currents. **E.**
786 Representative traces of hypertonic sucrose (0.5 M) used to elicit exocytosis of
787 releasable vesicles from neurons in the glucose control (black trace) and 2DG+oligo-
788 treated (blue trace) neurons. **F.** Summary of sucrose-elicited charge transfer from
789 glucose-treated ($n=5$ neurons) and 2DG+oligo-treated ($n=5$ neurons) cells ($p < 0.05$,
790 unpaired, two-tailed Student's t test). Individual data points represent single neurons,
791 bars represent mean \pm SEM. * $p \leq 0.05$. ** $p \leq 0.01$. *** $p \leq 0.001$.

792

793 **Figure 3.** Metabolically compromised neurons exhibit high variance in mPSC frequency
794 and display gradual, massive exocytosis. **A-C.** Representative traces of the indicated
795 experimental conditions, drug concentrations as in Figures 1 and 2. Examples B and C

796 represent different cells in the same condition with different spontaneous mPSC release
797 frequency. **D.** Summary of pooled mPSC frequency in the two conditions, revealing the
798 higher variance in mPSC frequency in 2DG+oligo (n=21, 22 neurons in glucose and
799 2DG+oligo conditions, respectively; $p=0.0002$, *F*-test). The difference between
800 conditions was not significantly different ($p > 0.05$, unpaired, two-tailed Student's *t*-test
801 with Bonferroni corrections). **E-G.** Summary of mPSC parameters, separated by
802 mEPSCs (n=9, 7 neurons in glucose and 2DG+oligo conditions, respectively) and
803 mIPSCs (n=8, 8 neurons in glucose and 2DG+oligo conditions, respectively). No
804 significant differences were found on any of the parameters between glucose and
805 2DG+oligo ($p > 0.05$, unpaired, two-tailed Student's *t*-test with Bonferroni corrections).
806 **H, I.** Representative traces documenting the effect of control (glucose) or 2DG+oligo
807 application on evoked and spontaneous release during recordings from a neuron on a
808 multi-neuron island. During recordings in TTX, K^+ was applied as in Figure 2 to elicit
809 transmitter release from surrounding terminals. Shown are antagonist-subtracted
810 currents at baseline (black) and following 15 min of control or 2DG+oligo application. **J.**
811 Summary of the change in total antagonist-subtracted (receptor-generated) charge
812 following 15 min incubation. Some depression in control K^+ -evoked PSCs (n = 7) was
813 noted. However, 2DG+oligo (n = 6) caused a complete loss of evoked PSC. A repeated
814 measures ANOVA revealed a significant interaction between treatment condition and
815 time ($*p < 0.01$). **K, L.** mPSC recordings from the neurons shown in H and I. The traces
816 document mPSCs at three 30-s epochs following the baseline K^+ application, as labeled.
817 Initially (time =0), mPSC frequency is high in both cells, a residual effect of K^+
818 application. **M.** Summary of mPSC frequency change from 30-s epochs during
819 incubation in 2DG+oligo. Same 13 cells represented in panel J. 2DG+oligo elicited a
820 significantly more sustained mPSC frequency than control ($*p < 0.005$ main effect of
821 treatment and interaction between time and treatment). **N-P.** The increased mPSC

822 frequency increase was not the result of interaction with K^+ stimulation. **N,O.** Sample
823 records from control and poisoned neurons, without preceding K^+ stimulation. **P.**
824 Summary data from multiple cells at early and late time points. A two-way, repeated-
825 measures ANOVA revealed a main effect of poison and a drug by time interaction
826 ($p < 0.05$). Asterisks indicate Bonferroni corrected post-hoc testing, **** $p \leq 0.0001$. n.s.,
827 not significant. Individual data points represent neurons, and bars represent mean \pm
828 SEM.

829

830

831 **Figure 4.** Synaptic vesicle cycling is impaired following combined inhibition of glycolysis
832 and oxidative phosphorylation. **A.** Representative images of presynaptic terminals
833 immunopositive for synapsin I (left, magenta) after induced vesicle cycling in the
834 presence of FM1-43FX (center, green), and merged (right, white) showing the
835 internalization of FM1-43FX during vesicle endocytosis in the presence of glucose. **B–F.**
836 Example merged images after 20 min pre-incubation in solution containing 45 mM KCl
837 (B), 2DG (C), oligo (D), 2DG+oligo (E), or 0 mM Ca^{2+} (F). **G.** Summary of cycling (A; n
838 =150 presynaptic terminals for each condition from three replications). Scale bar, 10 μ m.
839 * $p < 0.05$ for all the comparisons between each of the 45 mM KCl, 2DG, and oligo
840 conditions and either the 2DG+oligo or 0 mM Ca^{2+} condition (45 mM KCl vs. 2DG +
841 oligo, $p = 0.0127$; 2DG vs. 2DG+oligo, $p < 0.0001$; oligo vs. 2DG + oligo, $p = 0.0026$; 45
842 mM KCl vs. 0 mM Ca^{2+} , $p < 0.0001$; 2DG vs. 0 mM Ca^{2+} , $p < 0.0001$; oligo vs. 0 mM
843 Ca^{2+} , $p < 0.001$). The 2DG+oligo condition was not significantly different from the 0 mM
844 Ca^{2+} condition (NS, $p = 0.0746$, Kruskal-Wallis one-way ANOVA followed by Dunn's
845 multiple comparisons test). Data are represented as mean \pm SEM. * $p \leq 0.05$. n.s., non-
846 significant.

847

848 **Figure 5.** Endocytosis is inhibited during metabolic arrest despite continued exocytosis.
849 FM1-43FX incubation occurred during 20 min glucose (control), sustained
850 depolarization, or 2DG+oligo. **A.** Representative images show merged fluorescence of
851 synapsin labeling (magenta) and FM1-43 uptake (green). Scale bar 10 μm . **B.** Summary
852 of 150 terminals from 3 independent experiments reveals that while continued cycling is
853 evident with sustained depolarization, FM1-43 uptake is lost during metabolic arrest,
854 despite strong, prolonged exocytosis evident in Figure 3 (** $p < 0.001$)

855

856 **Figure 6.** Oxidative phosphorylation plays a privileged role in recovery from intense
857 presynaptic activity. **A.** Schematic and representative data showing autaptic EPSCs
858 evoked by action potentials in normal glucose solution before (left) and after (right)
859 vesicle depletion with strong, sustained depolarization with 90 mM K^+ for 30 sec.
860 Stimulus action currents in this figure and subsequent figures are blanked for clarity. **B,**
861 **C.** Representative recovery traces from 2DG (B) and oligo alone (C) treatments,
862 showing poor recovery from vesicle depletion in the oligo alone condition. **D, E.**
863 Summary of recovery of action potential-evoked EPSCs following the depletion protocol
864 for 2DG compared to glucose control (D, $P > 0.05$, two-way ANOVA), and glucose saline
865 in the presence (+oligo) or absence (-oligo) of 1 μM oligomycin (E, $p < 0.05$ two-way
866 ANOVA). **F, G.** Summary of axosomatic sodium currents following the depletion protocol
867 for 2DG compared to glucose control (F, $p > 0.05$, two-way ANOVA), and glucose saline
868 in the presence or absence of oligomycin (G, $p > 0.05$, two-way ANOVA). Data are
869 represented as mean \pm SEM. * $p \leq 0.05$. n.s, non-significant.

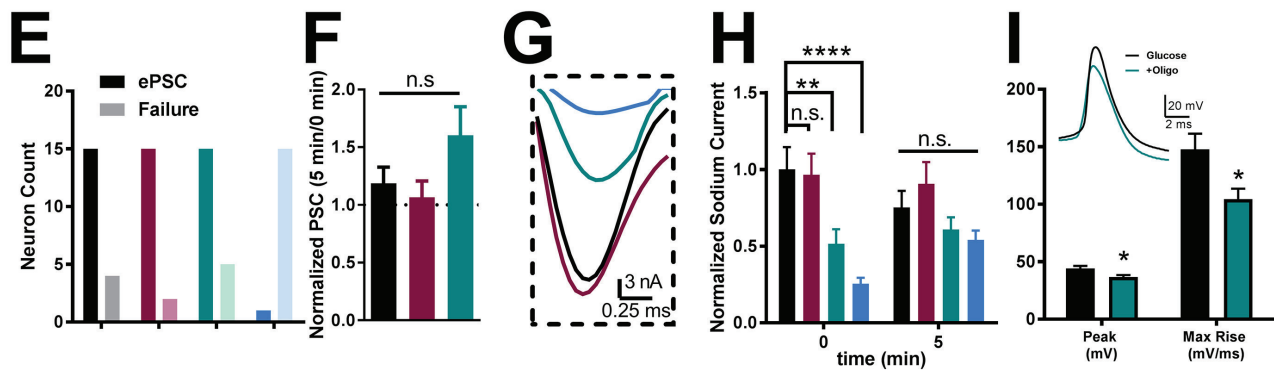
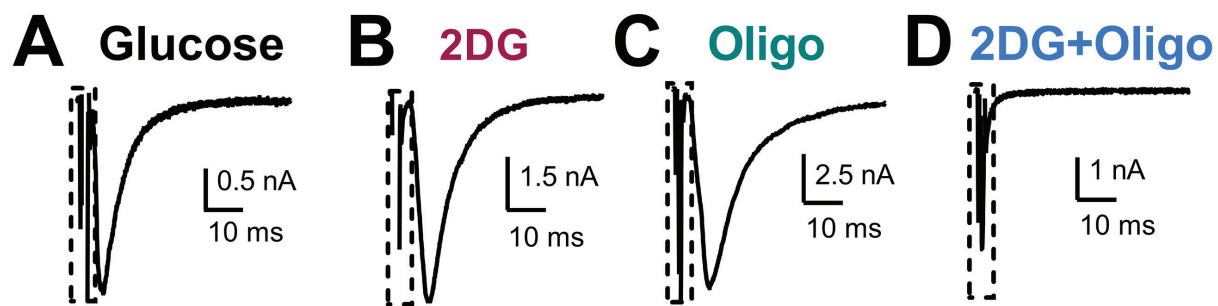
870

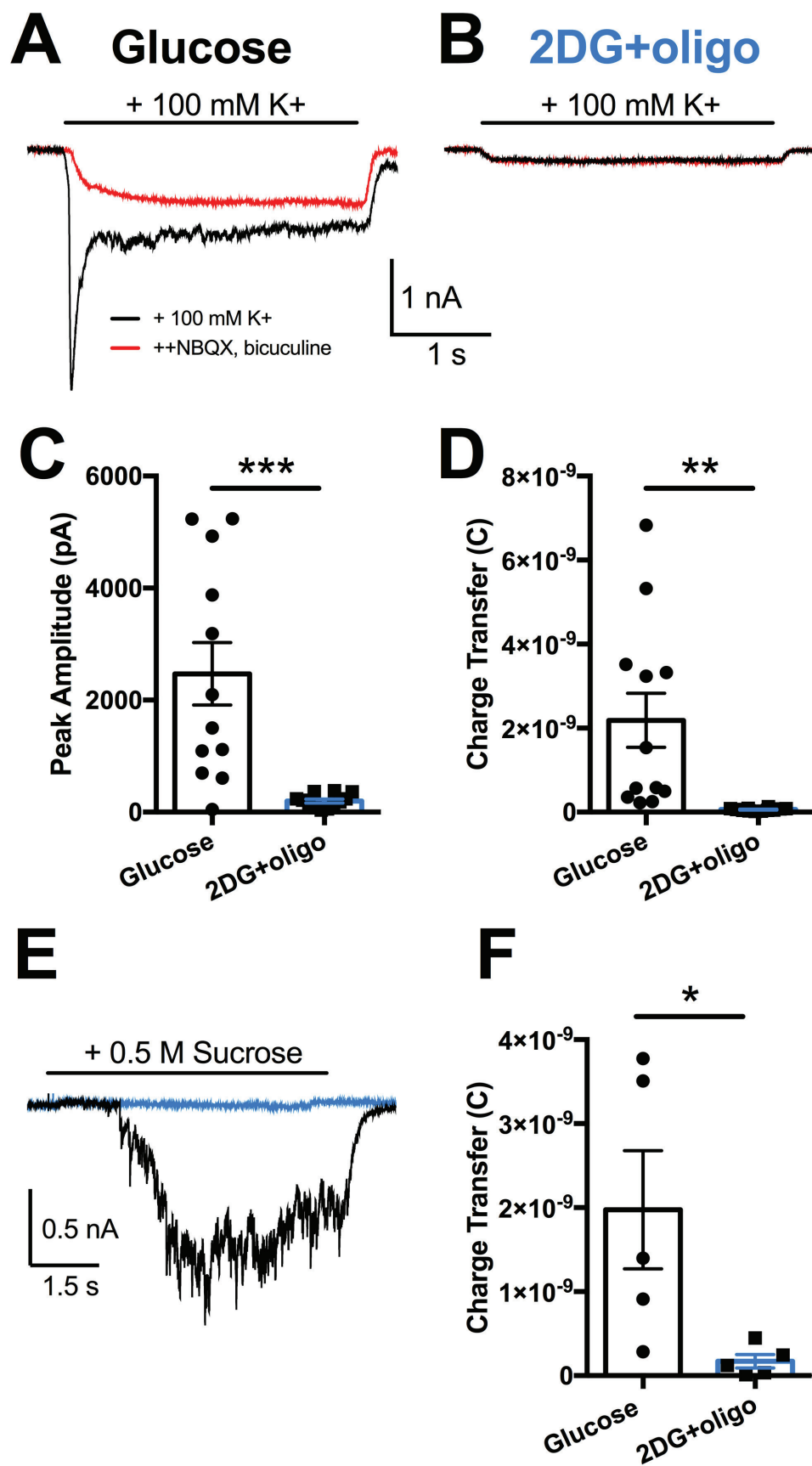
871 **Figure 7.** Local, on-demand monocarboxylate shuttling does not support the oxidative
872 phosphorylation required for recovery. **A, B.** Recovery of evoked EPSCs after 30 sec of
873 90 mM K^+ from microcultures containing (+astrocyte) or missing (-astrocyte) a local

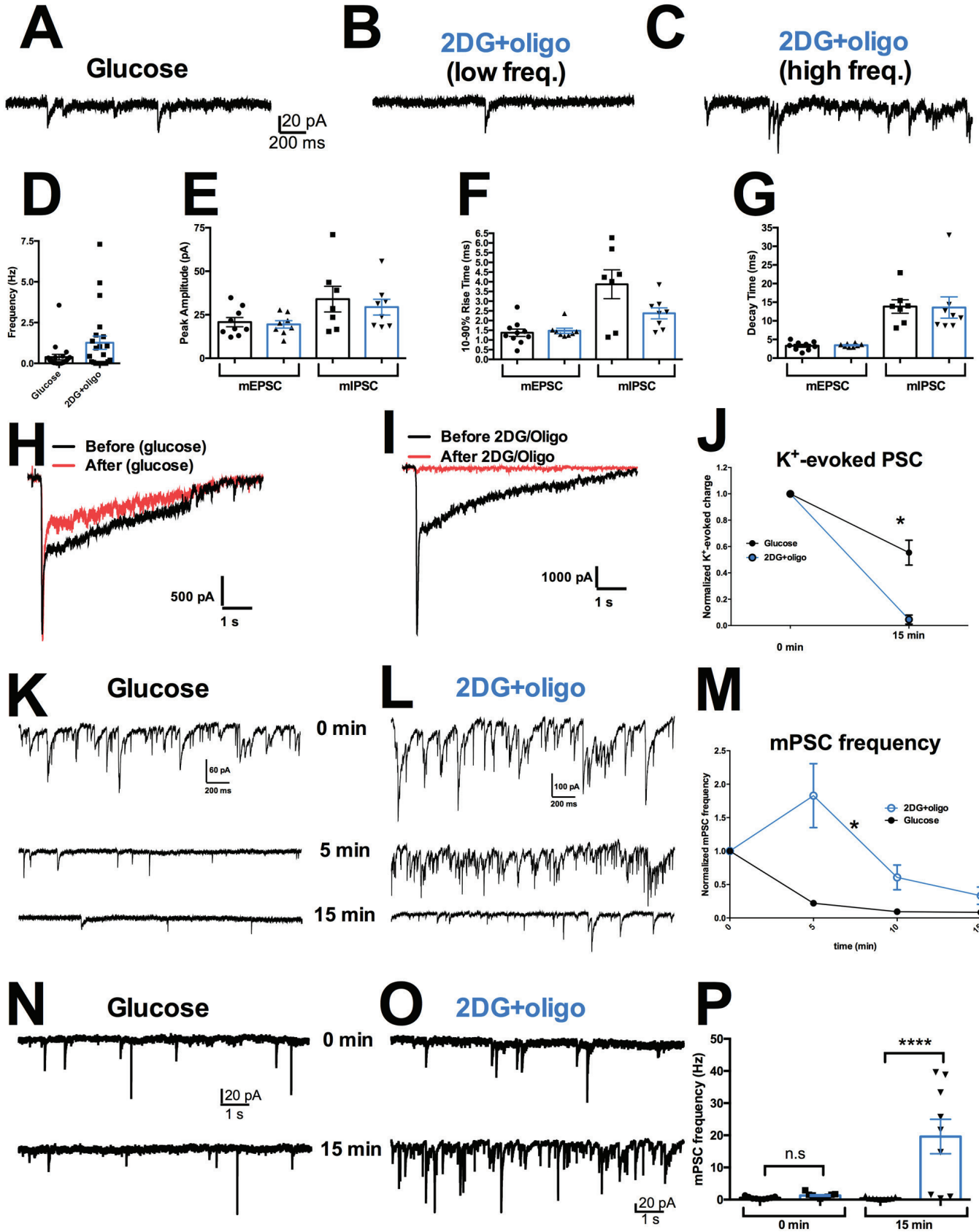
874 astrocyte bed. Note that both +astrocyte and -astrocyte microcultures were obtained
875 from the same plates. **C.** Summary of recovery following vesicle depletion in +astrocyte
876 (black) and -astrocyte (red) microcultures ($p > 0.05$, two-way ANOVA). **D.** Summary of
877 recovery of sibling -astrocyte EPSCs incubated in control medium (light red) or in lactate
878 (dark red, 1.5 mM, 15 min; $p > 0.05$, two-way ANOVA). Data are represented as mean \pm
879 SEM. n.s, non-significant.

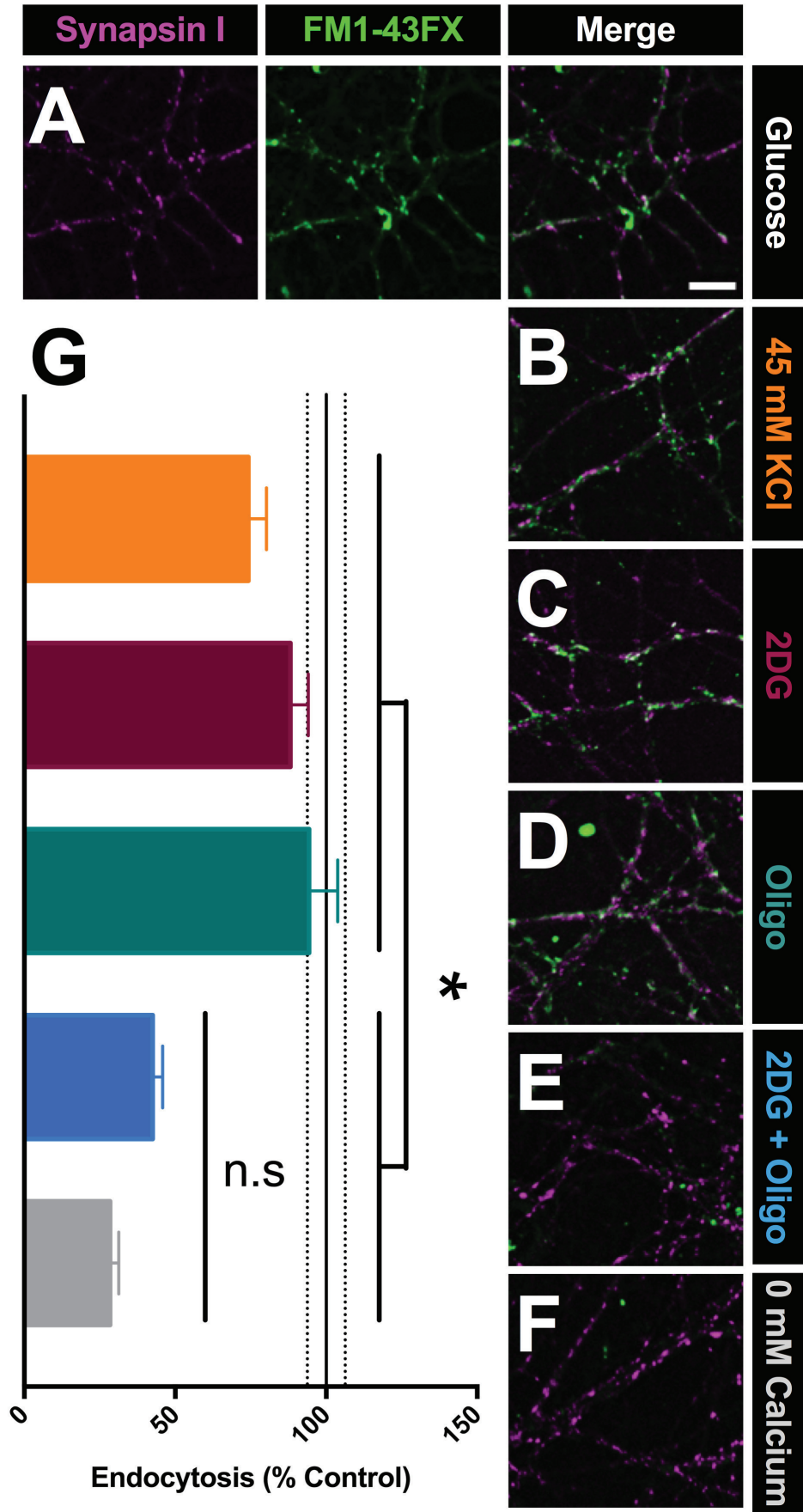
880

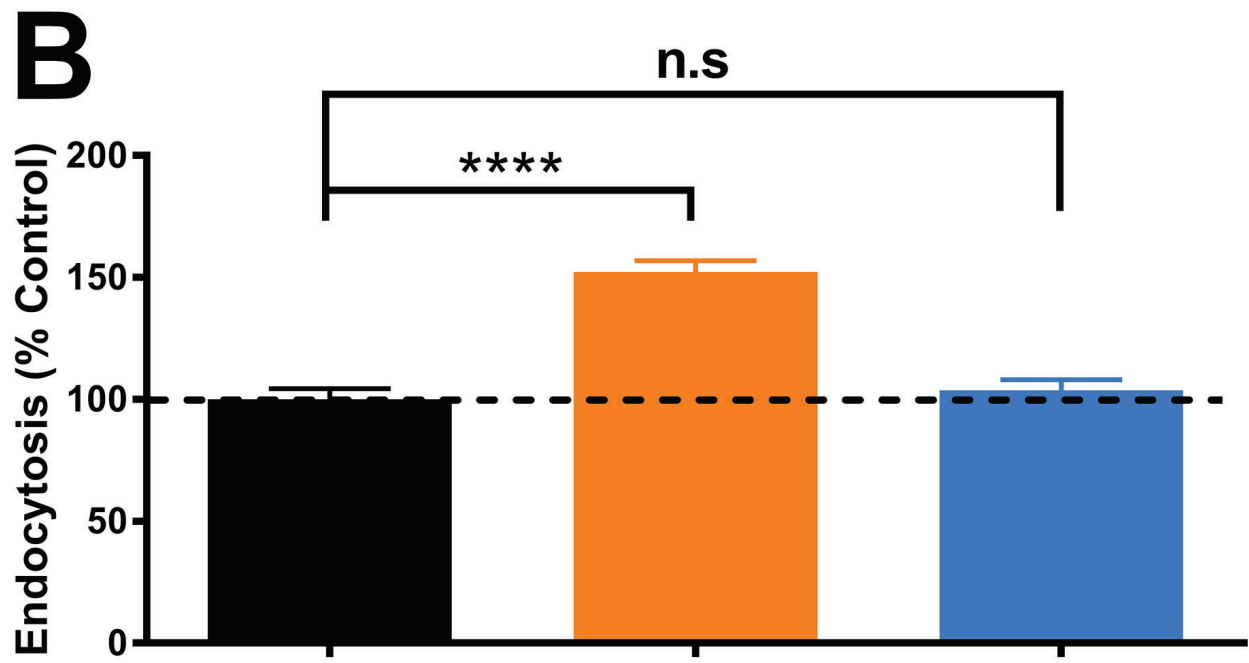
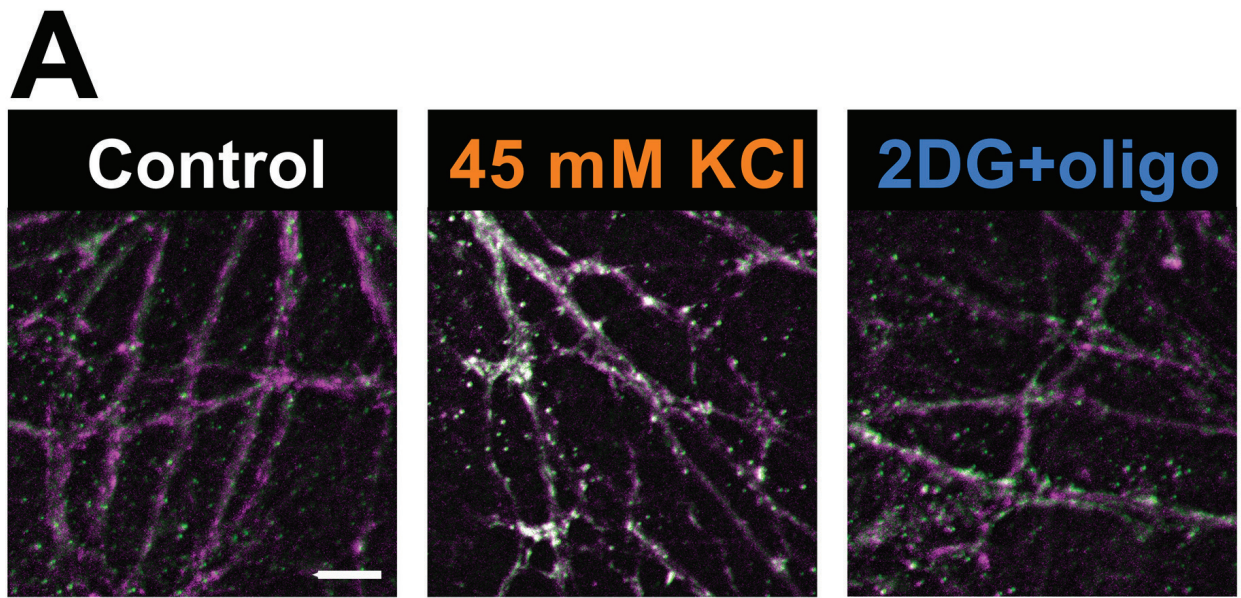
881 **Figure 8.** Oxidative phosphorylation fueling presynaptic recovery is flexibly supplied by
882 neuronal glycolysis or by monocarboxylate transport. **A, B.** Representative traces of
883 EPSC recovery following monocarboxylate transport inhibition alone (A; 4-CIN, 100 μ M)
884 or combined inhibition of glycolysis and monocarboxylate transport (B; 2DG+4-CIN) for
885 15 min. **C, D.** Summary of recovery after 30 sec of 90 mM K^+ following incubation in 4-
886 CIN alone (C, $p > 0.05$, two-way ANOVA) or combined 2DG+4-CIN (D, $p < 0.05$, two-
887 way ANOVA). Data are represented as mean \pm SEM. * $p \leq 0.05$. n.s, non-significant

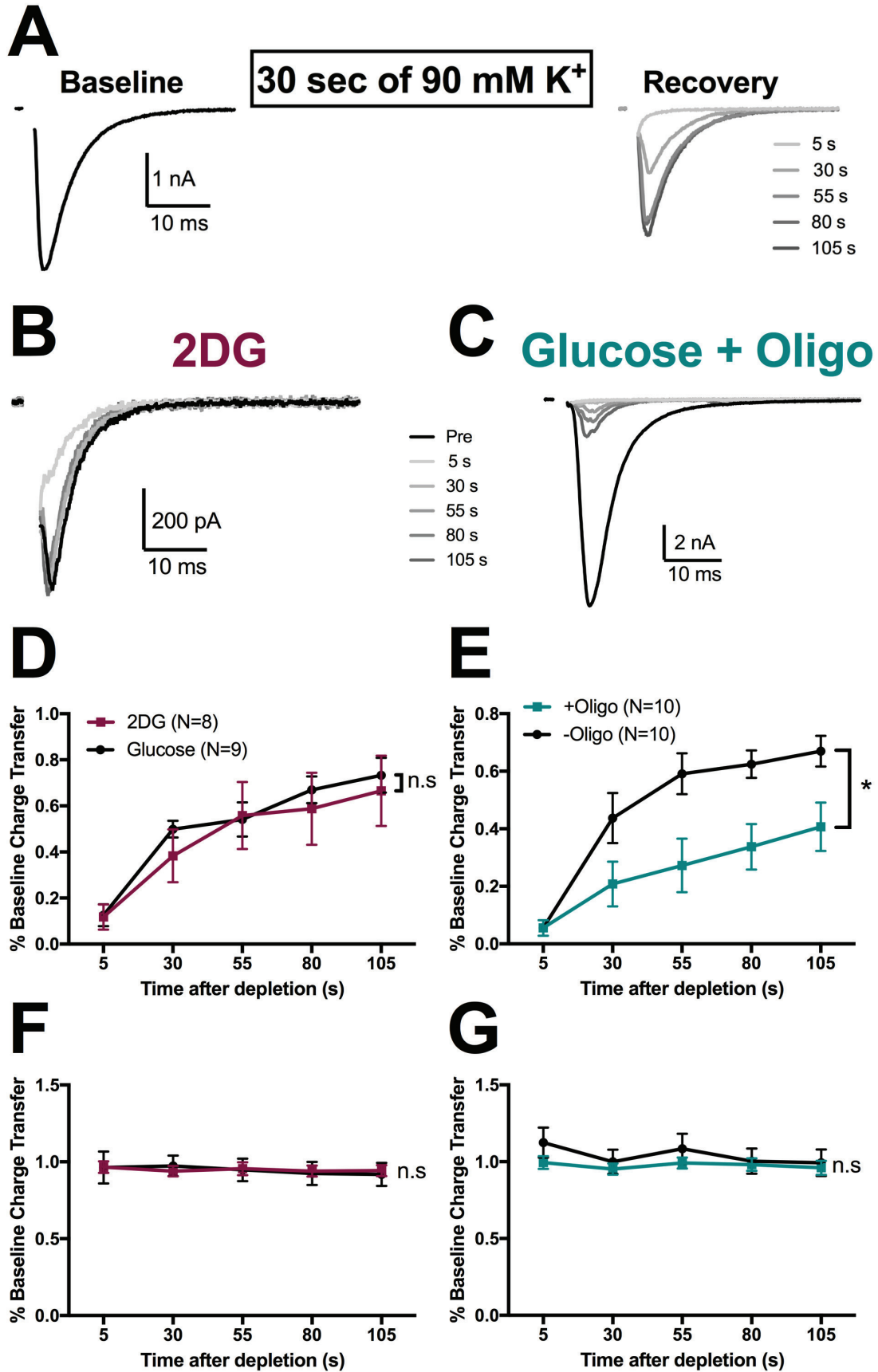


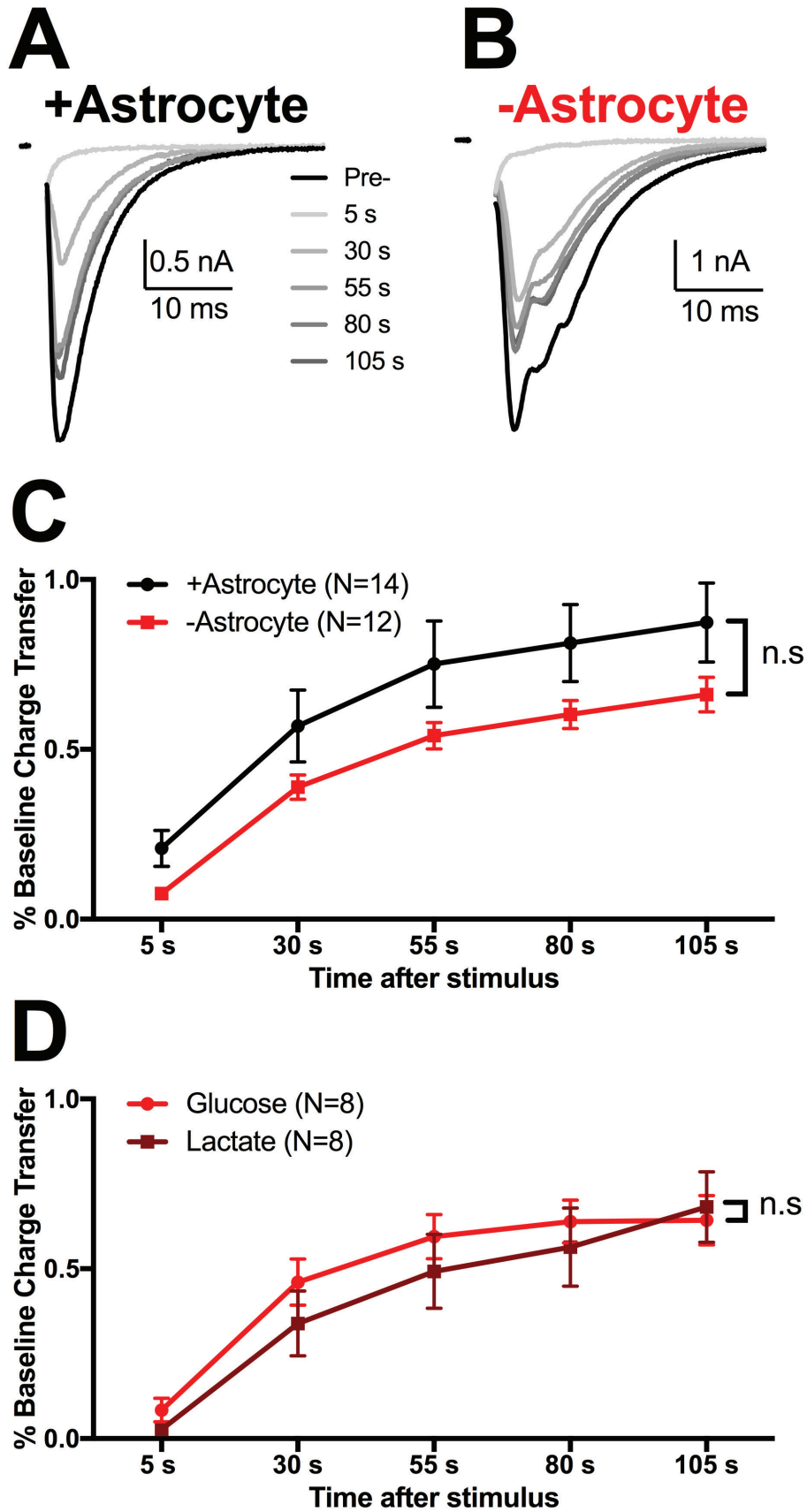




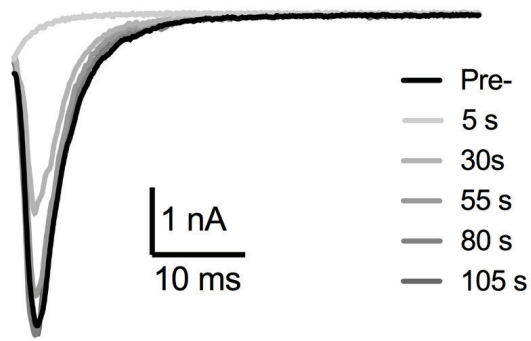








A Glucose + 4-CIN



B 2DG + 4-CIN

